
Candidate Set Re-ranking for Composed Image Retrieval with Dual Multi-modal Encoder

Zheyuan Liu

Australian National University
zheyuan.liu@anu.edu.au

Weixuan Sun

Australian National University
weixuan.sun@anu.edu.au

Damien Teney

Idiap Research Institute
damien.teney@idiap.ch

Stephen Gould

Australian National University
stephen.gould@anu.edu.au

Abstract

Composed image retrieval aims to find an image that best matches a given multi-modal user query consisting of a reference image and text pair. Existing methods commonly pre-compute image embeddings over the entire corpus and compare these to a reference image embedding modified by the query text at test time. Such a pipeline is very efficient at test time since fast vector distances can be used to evaluate candidates, but modifying the reference image embedding guided only by a short textual description can be difficult, especially independent of potential candidates. An alternative approach is to allow interactions between the query and every possible candidate, i.e., reference-text-candidate triplets, and pick the best from the entire set. Though this approach is more discriminative, for large-scale datasets the computational cost is prohibitive since pre-computation of candidate embeddings is no longer possible. We propose to combine the merits of both schemes using a two-stage model. Our first stage adopts the conventional vector distancing metric and performs a fast pruning among candidates. Meanwhile, our second stage employs a dual-encoder architecture, which effectively attends to the input triplet of reference-text-candidate and re-ranks the candidates. Both stages utilize a vision-and-language pre-trained network, which has proven beneficial for various downstream tasks. Our method consistently outperforms state-of-the-art approaches on standard benchmarks for the task.

1 Introduction

The task of composed image retrieval aims at finding a candidate image from a large corpus that best matches a user query, which is comprised of a reference image and a modification sentence describing certain changes. Compared to conventional image retrieval setups such as text-based [25] or content-based [38] retrieval, the incorporation of both the visual and textual modalities enables users to more expressively convey the desired concepts, which is useful for both specialized domains such as fashion recommendations [13, 14] and the more general case of searching over open-domain images [8, 9, 28].

Existing work [3, 5, 11, 28, 40] on composed image retrieval mostly adopts the paradigm of separately embedding the input visual and textual modalities, followed by a model that acts as an image feature modifier conditioned on the text. The modified image feature is finally compared against features of all candidate images through a vector distance (e.g., cosine similarity) before yielding the most similar one as the prediction (see Figure 1 (left)). The main benefit of such a pipeline is the inference cost. Let us assume that a corpus \mathcal{D} contains M candidate images. For a query pair of reference image I_R and

modification text t , to select the best matching candidate, the model shall exhaustively assess triplets $\langle (I_R, t), I_C \rangle$ for every image $I_C \in \mathcal{D}$. Existing pipelines individually pre-embed all candidate images to compare with the joint-embedded of (I_R, t) computed on the fly, where the comparison can be done very quickly. We point out that the above pipeline presents a trade-off between the inference cost and the ability to exercise explicit text-image interactions for each candidate. In essence, candidate images are only presented to the model indirectly through the loss function, resulting in the model having to estimate the modified visual features from text inputs in its forward path.

Here, we propose an alternative solution that exhaustively classifies triplets with query-specific candidate features, which achieves appreciable performance gain while still maintaining a reasonable inference cost. We observe that for composed image retrieval, easy and hard negatives can be distinctly separated. As the nature of this task dictates that the ground truth candidate be visually similar to the reference, otherwise it would be trivial to study a modification [8, 28]. We can further deduce that a group of hard negatives exist, which is likely to benefit from fine-grained multi-modal reasoning. This observation motivates a two-stage method, where we first filter all candidates to reduce their quantity. Since the goal at this stage is oriented toward removing easy negatives, a low-cost vector distance-based pipeline would suffice. We then re-rank the remaining candidates with explicit text-image matching on each possible triplet. Granted, such a process is more computationally intense but is empirically beneficial for reasoning among hard candidates. With the pre-filtering in place, we are able to limit the overall inference time within an acceptable range. The main focus of this paper is on the second stage.

Note that our two-stage pipeline relates to the inference scheme of image-text retrieval [27] in recent Vision-and-Language Pretrained (VLP) networks [22, 23]. Specifically, Li et al. [22] propose to first compute feature similarities for all image-text pairs, then re-rank the top- k candidates through a joint image-text encoder via the Image-Text Matching (ITM) scores, which greatly speeds up the inference compared to previous VLP networks that require computing ITM scores for *all* image-text pairs [6, 26]. Here, we arrive at a similar two-stage scheme but for the task of composed image retrieval. We also note that our method, although sharing a similar philosophy and is based on VLP networks, is not a direct replica of what is done in the image-text retrieval tasks discussed above. With the unique input triplets of $\langle (I_R, t), I_C \rangle$, novel model architectures are required for efficient interactions among the three features of two modalities.

In summary, our contribution is a two-stage method that combines the efficiency of the existing pipeline and the ability to assess fine-grained query-candidate interactions through explicit pairing. We base our design on VLP models while developing task-specific architectures that encourage interactions among input entities. Our approach significantly outperforms existing methods on datasets of multiple domains.

2 Related Work

The task of image retrieval traditionally accepts input in the form of either an image [38] or text [25, 44]. The aim is to retrieve an image whose content is the most similar to the input one, or respectively, best matches the textual description. Vo et al. [40] propose composed image retrieval, which takes as input both modalities, using an image as a reference while text as a modifier.

Current approaches address this task by designing models that serve as a reference image modifier conditioned on text, essentially composing the input modalities into one joint representation, which is compared with features of candidates through, e.g., cosine similarity. Among them, TIRG [40] uses a gating mechanism along with a residual connection that aims at finding relevant changes and preserving necessary information within the reference respectively. The outputs of the two paths are summed together to produce the final representation. Anwaar et al. [2] follow a similar design but pre-encode the inputs separately and project them into a common embedding space for manipulation. Hosseinzadeh and Wang [16] propose to adopt regional features as in VQA [1] instead of CNN features. Likewise, Wen et al. [41] develop global and local composition networks to better fuse the modalities. VAL [5] introduces a transformer network to jointly encode the input modalities, where the hierarchical design encourages multi-layer matching. MAAF [11] adopts the transformer network differently by pre-processing the input into sequences of tokens to be concatenated and jointly attended. Yang et al. [42] designs a joint prediction module on top of VAL that highlights the correspondences between reference and candidate images. Notably, the module is only used in

training as it is intractable to apply it to every possible pair of reference and candidate images during inference. CIRPLANT [28] proposes to use a pre-trained vision-and-language (VLP) transformer to modify the visual content, alongside CLIP4CIR [3, 4], BLIP4CIR [29] and CASE [21].

DCNet [18] introduces the Composition and Correction networks, with the latter accepting a reference image with a candidate target image and assesses their relevancy. This, on first look, suggests an exhaustive reference-candidate pairing. Though, inference cost limits the interaction of a pair of reference and candidate images to simple operations — i.e., element-wise product and subtraction with a single-layer MLP. ARTEMIS [9] is the first to introduce a model that scores each triplet of query and candidate image, which separates it apart from an image modifier-based pipeline. However, inference cost still confines such scoring to cosine similarities between individually pre-encoded modalities. In contrast to existing approaches, our method is in two stages. We do not seek to modify image features in an end-to-end manner. Instead, we pre-filter the candidates and focus more on re-ranking the hard negatives. The re-ranking step is formatted as a scoring task based on contrastive learning, which is natural for VLP networks trained with similar objectives.

We note that the concept of a two-stage scheme is not new for conventional image-text or document retrieval. Indeed, re-ranking a selected list of candidate images via e.g., k -nearest neighbors [36] or query expansion techniques [7] has been widely studied. More recent and related work on VLP models [22–24] propose to first score the similarities between image and text features, then re-rank the top- k pairs via a multi-modal classifier. This aligns nicely with the two pre-training objectives, namely, Image-Text Contrastive and Image-Text Matching. To the best of our knowledge, we are the first to apply such a two-stage scheme to composed image retrieval. We contribute by designing an architecture that reasons over the triplet of $\langle (I_R, t), I_C \rangle$, which differs from the conventional retrieval tasks discussed above.

3 Two-stage Composed Image Retrieval

Composed image retrieval can be defined as follows. Let I_R be some reference image and t be a piece of text describing a change to the image. Then given a query consisting of the pair $q = (I_R, t)$, the aim of composed image retrieval is to find the best match, i.e., the target image I_T , among all candidates in a large image corpus \mathcal{D} . In this work, we propose a two-stage model where we first filter the large corpus to obtain a smaller set of candidate images relevant to the query (see Section 3.1), and then re-rank to obtain an ordered list of target images (see Section 3.2).

For both steps, we base our designs on the pre-trained vision-and-language (VLP) network BLIP [23], though other VLP models might be used. BLIP consists of an image encoder and a text encoder. The image encoder is a vision transformer [12] that accepts as input a raw image and produces the spatial image features by slicing the image in patches and flattening them in a sequence. A global image feature is also represented as a prepended special [CLS] token. The text encoder can operate in three modes. When configured as a uni-modal encoder, it takes in a sequence of tokenized words from a text sequence and outputs the sequential features with a [CLS] token summarizing the whole text, as in BERT [10]. Optionally, the text encoder can be configured as a multi-modal encoder, where a Cross-Attention (CA) layer is inserted after each Self-Attention (SA) layer. As shown in Figure 2, the CA layer accepts the sequential output of the image encoder and performs image-text attention. The output of which is passed into the Feed-Forward (FF) layer and is the same length as the input text sequence. The transformer-based text encoder accepts inputs of varied lengths while sharing the same token dimension d as the output of the image encoder. In this paper, we denote the features of an arbitrary image (resp. input text) as v (resp. w) and its length as L_v (resp. L_w). We note that a decoder mode is also available in BLIP for generative tasks (e.g., image captioning [1]), though it is not used in this work.

3.1 Candidate Filtering

The first stage of our approach aims to filter out the majority of candidates leaving only a few of the more difficult candidates for further analysis in the second step. Shown in Figure 1 (left), we adopt the BLIP text encoder in its multi-modal mode such that it jointly embeds a given query $q = (I_R, t)$ into a sequential output, which we denote as $z_t \in \mathbb{R}^{L_w \times d}$. We extract the feature of the [CLS] token in z_t as a single d -dimensional vector and compare it to pre-computed [CLS] embeddings of all candidate images $I'_i \in \mathcal{D}$ via cosine similarity. Note that the pre-computed candidate embeddings

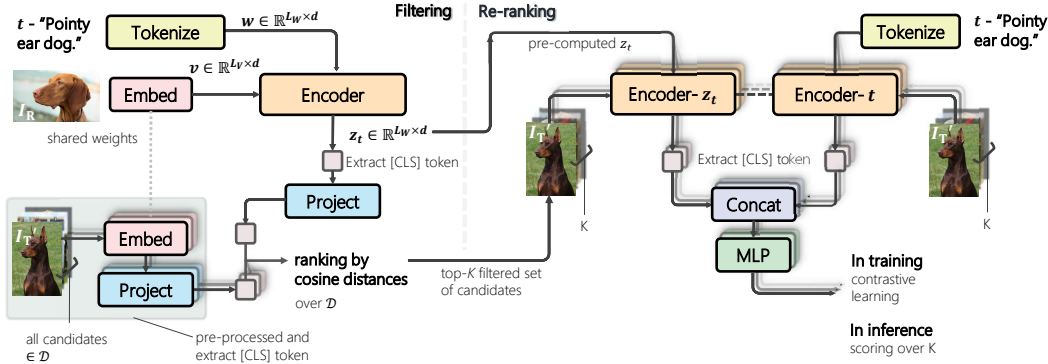


Figure 1: Overall training pipeline. **Left:** Candidate Filtering model, which takes as input the tokenized text and cross-attends it with the reference image. The output is the sequential feature z_t , where we extract the [CLS] token as the summarized representation of the query $q = (I_R, t)$ to compare its similarity with features of I_T' . **Right:** Candidate Re-ranking model with dual-encoder architecture. Stacked elements signify that we exhaustively pair up each candidate I_T' among the selected top- K with the query q for assessment. Note that the two encoders take in different inputs for cross-attention. The output [CLS] tokens are concatenated and passed for producing a logit.

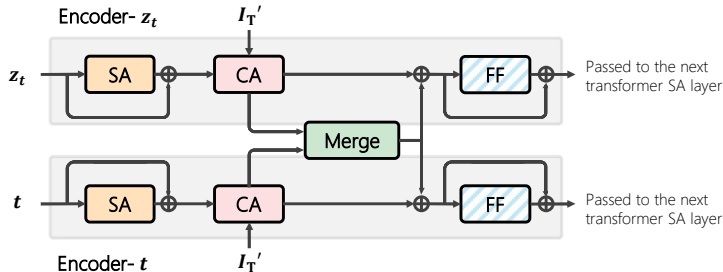


Figure 2: Details of the transformer layer in our dual-encoder architecture. Here, we take the first layer as an example. **SA:** Self-Attention layer, **CA:** Cross-Attention layer, **FF:** Feed-Forward layer. \oplus : element-wise addition for residual connections. Dashed fillings on FF suggest weight-sharing.

are independent of the query text, a weakness that we address in our second stage model. Since BLIP by default projects the [CLS] token features into $d = 256$ for both image and text, the comparison can be efficiently done through a cosine similarity.

After training the candidate filtering model, we select the top- K candidates (for each query) for re-ranking in the second stage. Here we choose K to be sufficiently large so that the ground-truth target is within the selected images for most queries. We term the percentage value of queries with ground truth within the top- K as *ground truth coverage* in the following sections. Empirically, we find that setting K to 50 or 100 gives a good trade-off between recall and inference cost in the second stage. Details on the ablation of K across datasets are discussed in Section B.1.

We note that concurrent to our work, CASE [21] adopts a similar approach as our Candidate Filtering model, in that it uses BLIP for reference image-text fusion. We point out that both our filtering model and CASE use BLIP in one of its originally proposed configurations without architectural changes, and hence, is unsurprising and could be viewed as a natural progression for the task. Meanwhile, our second-stage re-ranking sets us apart from this concurrent work.

3.2 Candidate Re-ranking

The second stage re-ranks the filtered set of candidates. Since this set is much smaller than the entire corpus we can afford a richer, more expensive approach. To this end, we introduce a novel dual-encoder design for this subtask inspired by the BLIP architecture proposed for NLVR [37].

As shown in Figure 1 (right), our two encoders run in parallel as two branches to serve separate purposes, one to encode I_R with I'_T and the other to encode t with I'_T . Internally, they exchange information via dedicated merging layers. Encoder- z_t , as the name suggests, accepts as input $z_t \in \mathbb{R}^{L_w \times d}$ from the previous stage. Since we do not further finetune the Candidate Filtering model in the second stage, z_t can be precomputed for each query of $q = (I_R, t)$. Meanwhile, Encoder- t takes as input the tokenized t , which is then embedded into a sequential feature of size $\mathbb{R}^{L_w \times d}$. Here, note that for a given query, the lengths of z_t and the embedded t are always identical, as the output of a text encoder (i.e., the Candidate Filtering model) shall retain the dimension of the input coming through the SA layers (see Figure 2). This characteristic makes merging the outputs of the two encoders within each transformer layer effortless.

We use a default 12-layer transformer for each encoder. Within each transformer layer, both encoders cross-attend the inputs introduced above with the sequential feature of an arbitrary I'_T . The intuition is to allow I'_T to separately attend to the two elements in each query q for relevancy, namely t and I_R . For Encoder- t , the two entities entering the CA layer are self-explanatory. However, for Encoder- z_t , we opt for using z_t as a surrogate of I_R . The main reason is the GPU memory limit, as it is intractable to perform image-image cross attention with the default $L_v = 577$ during training. Although spatial pooling can be used to reduce the length of the input I_R sequence, we empirically find it inferior, potentially due to the loss of information in pooling. Details are discussed in Section 4.3. On the other hand, z_t can be viewed as an embedding that contains sufficient I_R information and is readily available, as it has been pre-computed in the previous stage from the query pair q . A bonus of using z_t is that we can easily merge the cross-attended features, since it shares the same dimensionality as t at all times. Empirically, we confirm that our design choices yield a better result.

Figure 2 depicts the transformer block of the re-ranking model. As illustrated, we merge the outputs of the CA layers from the two encoders in each transformer layer. Specifically, given the outputs of the encoders after the CA layers, the merging is performed as an average pooling in the first six layers, and a concatenation followed by a simple MLP in the last six layers. The merged feature is then passed into a residual connection, followed by the FF layers. Regarding weight-sharing across layers in each encoder, we opt for having separate weights of SA and CA layers within each encoder, while sharing the weights of FF layers to account for the different inputs passing through the SA and CA layers. We point out that due to the residual connections (Figure 2), the outputs of the two encoders after the final transformer block are different in values, even though the FF layers are of the same weights.

We formulate the re-ranking as a scoring task—among the set of candidate images score the true target higher than all other negative images. For each sequential output from either encoder, we extract the [CLS] token at the front as the summarized feature. We then concatenate the two [CLS] outputs from two encoders and use a two-layer MLP as the scorer head, which resembles the BLIP Image-Text Matching task setup.

3.3 Training Pipeline

Candidate Filtering. Our filtering model follows the contrastive learning pipeline [33] with a batch-based classification loss [40] commonly adopted in previous work [21, 29]. Specifically, in training, given a batch size of B , the features of the i -th query (I_R^i, t^i) with its ground-truth target I_T^i , we formulate the loss as:

$$\mathcal{L}_{\text{Filtering}} = -\frac{1}{B} \sum_{i=1}^B \log \left[\frac{\exp \left[\lambda \cdot \kappa \left(f_{\theta} \left(I_R^i, t^i \right), I_T^i \right) \right]}{\sum_{j=1}^B \exp \left[\lambda \cdot \kappa \left(f_{\theta} \left(I_R^i, t^i \right), I_T^j \right) \right]} \right], \quad (1)$$

where f_{θ} is the Candidate Filtering model parameterized by θ , λ is a learnable temperature parameter following [33], and $\kappa(\cdot, \cdot)$ is the similarity kernel as cosine similarity.

In inference, the model ranks all candidate images I'_T for each query via the same similarity kernel $\kappa(\cdot, \cdot)$. We then pick the top- K lists for each query for the second-stage re-ranking.

Candidate Re-ranking. The re-ranking model is trained with a similar contrastive loss as discussed above. Specifically, for each $\langle (I_R^i, t^i), I_T^i \rangle$ triplet, we extract the predicted logit and contrast it against

all other $\langle (I_R^i, t^i), I_T^j \rangle$ with $i \neq j$, essentially creating $(B - 1)$ negatives for each positive triplet. The loss is formulated as:

$$\mathcal{L}_{\text{Re-ranking}} = -\frac{1}{B} \sum_{i=1}^B \log \left[\frac{\exp[f_\gamma(I_R^i, t^i, I_T^i)]}{\sum_{j=1}^B \exp[f_\gamma(I_R^i, t^i, I_T^j)]} \right], \quad (2)$$

where f_γ is the Candidate Re-ranking model parameterized by γ .

Note that in training, we randomly sample negatives within the same batch to form triplets. Therefore, the choice of K does not affect the training process. We empirically find this yielding better performance than training only on the top- K negatives, with the benefit of not relying on a filtered candidate list for training. Incidentally, it is also more efficient, as we do not need to independently load negatives for each query. During inference, the model only considers, for each query, the selected top- K candidates and ranks them by the predicted logits.

4 Experiments

4.1 Experimental Setup

Datasets. Following previous work, we consider two datasets in different domains. Fashion-IQ is a dataset of fashion products in three categories, namely *Dress*, *Shirt*, and *Toptee*, which form over 30k triplets with 77k images. The annotations are collected from human annotators and are overall concise. CIRR [28] is proposed to specifically study the fine-grained visiolinguistic cues and implicit human agreements. It contains 36k pairs of queries with human-generated annotations, where images often contain rich object interactions [37]¹.

Evaluation Metrics. We follow previous work to report our results in Recall@ K , that is the percentage of queries whose true target is ranked to be among the top- K candidates. For Fashion-IQ, we assess the performance with Recall@10 and 50 on each category [13]. Such choices of K values account for the possible false negatives in the candidates. On CIRR, we report Recall@1, 5, 10, and 50. We additionally record Recall_{subset}@ K [28], where the candidates are limited to a pre-defined set of five with high similarities. The set of five candidates contains no false negatives, making this metric more suitable to study fine-grained reasoning ability.

For Fashion-IQ, we report results on the validation split, as the ground truths of the test split remain nonpublic. For CIRR, we report our main results on the test split obtained from the evaluation server².

Implementation Details. We adopt the standard image pre-processing and model configurations of BLIP encoders [23]. Except for image padding, which we follow Baldrati et al. [3] with a padding ratio of 1.25. We initialize the image and text encoders with the BLIP w/ ViT-B pre-trained weights. In both stages, we freeze the ViT image encoder and only finetune the text encoders due to the GPU memory limits. We follow BLIP downstream task settings and optimize with AdamW [30] with a cosine learning rate schedule. Training details for each dataset in the two stages are listed in Section A.

All experiments are conducted on a single NVIDIA A100 80G with PyTorch while enabling automatic mixed precision. We base our implementation on the BLIP codebase³.

4.2 Performance Comparison with State-of-the-Art

Fashion-IQ. Table 1 compares the performance on Fashion-IQ. We note that our re-ranking model (row 20) outperforms all existing methods consistently across three categories. Impressively, the performance increase is notable when compared to CASE (row 18), a method that also uses BLIP encoders. This suggests that our two-stage design, particularly the explicit query-specific candidate re-ranking, is beneficial to the task.

¹Both datasets are publicly released under the MIT License, which allows distributions and academic usages.

²https://cirr.cecs.anu.edu.au/test_process/

³<https://github.com/salesforce/BLIP>

Methods	Dress		Shirt		Toptee		Average		Avg.	
	R@10	R@50	R@10	R@50	R@10	R@50	R@10	R@50	Metric	
1	MRN [19]	12.32	32.18	15.88	34.33	18.11	36.33	15.44	34.28	24.86
2	FiLM [32]	14.23	33.34	15.04	34.09	17.30	37.68	15.52	35.04	25.28
3	TIRG [40]	14.87	34.66	18.26	37.89	19.08	39.62	17.40	37.39	27.40
4	Relationship [34]	15.44	38.08	18.33	38.63	21.10	44.77	18.29	40.49	29.39
5	CIRPLANT [28]	14.38	34.66	13.64	33.56	16.44	38.34	14.82	35.52	25.17
6	CIRPLANT w/OSCAR [28]	17.45	40.41	17.53	38.81	21.64	45.38	18.87	41.53	30.20
7	VAL w/GloVe [5]	22.53	44.00	22.38	44.15	27.53	51.68	24.15	46.61	35.40
8	CurlingNet [43]	24.44	47.69	18.59	40.57	25.19	49.66	22.74	45.97	34.36
9	DCNet [18]	28.95	56.07	23.95	47.30	30.44	58.29	27.78	53.89	40.84
10	CoSMo [20]	25.64	50.30	24.90	49.18	29.21	57.46	26.58	52.31	39.45
11	MAAF [11]	23.8	48.6	21.3	44.2	27.9	53.6	24.3	48.8	36.6
12	ARTEMIS [9]	25.68	51.25	28.59	55.06	21.57	44.13	25.25	50.08	37.67
13	SAC w/BERT [17]	26.52	51.01	28.02	51.86	32.70	61.23	29.08	54.70	41.89
14	AMC [45]	31.73	59.25	30.67	59.08	36.21	66.06	32.87	61.64	47.25
15	CLIP4CIR [4]	33.81	59.40	39.99	60.45	41.41	65.37	38.32	61.74	50.03
16	BLIP4CIR [29]	42.09	67.33	41.76	64.28	46.61	70.32	43.49	67.31	55.40
17	FAME-ViL [†] [15]	42.19	67.38	47.64	68.79	<u>50.69</u>	<u>73.07</u>	46.84	69.75	58.29
18	CASE [21]	<u>47.77</u>	<u>69.36</u>	<u>48.48</u>	<u>70.23</u>	50.18	72.24	<u>48.79</u>	<u>70.68</u>	<u>59.74</u>
19	Ours F	43.78	67.38	45.04	67.47	49.62	72.62	46.15	69.15	57.65
20	Ours R ₁₀₀	48.14	71.34	50.15	71.25	55.23	76.80	51.17	73.13	62.15

Table 1: Fashion-IQ, validation split. We report Average Metric ($Recall_{Avg}@10 + Recall_{Avg}@50$)/2 as in [13]. Rows 1-2 are cited from [13]. †: Methods trained with additional data in a multi-task setup. **F** (shaded) denotes Candidate Filtering model, **R**_K denotes Candidate Re-ranking model with results obtained on the top-*K* filtered results from **F**. For Fashion-IQ we use top-100, which has a ground truth coverage of 77.24%, 75.86% and 81.18% for dress, shirt and toptee categories respectively. Best numbers (resp. second-best) are in **black** (resp. underlined).

Methods	Recall@ <i>K</i>				Recall _{Subset} @ <i>K</i>			Avg.	
	<i>K</i> = 1	<i>K</i> = 5	<i>K</i> = 10	<i>K</i> = 50	<i>K</i> = 1	<i>K</i> = 2	<i>K</i> = 3	Metric	
1	TIRG [40]	14.61	48.37	64.08	90.03	22.67	44.97	65.14	35.52
2	TIRG+LastConv [40]	11.04	35.68	51.27	83.29	23.82	45.65	64.55	29.75
3	MAAF [11]	10.31	33.03	48.30	80.06	21.05	41.81	61.60	27.04
4	MAAF+BERT [11]	10.12	33.10	48.01	80.57	22.04	42.41	62.14	27.57
5	MAAF-IT [11]	9.90	32.86	48.83	80.27	21.17	42.04	60.91	27.02
6	MAAF-RP [11]	10.22	33.32	48.68	81.84	21.41	42.17	61.60	27.37
7	CIRPLANT [28]	15.18	43.36	60.48	87.64	33.81	56.99	75.40	38.59
8	CIRPLANT w/OSCAR [28]	19.55	52.55	68.39	92.38	39.20	63.03	79.49	45.88
9	ARTEMIS [9]	16.96	46.10	61.31	87.73	39.99	62.20	75.67	43.05
10	CLIP4CIR [4]	38.53	69.98	81.86	95.93	68.19	85.64	94.17	69.09
11	BLIP4CIR [29]	40.15	73.08	83.88	96.27	72.10	88.27	95.93	72.59
12	CASE [21]	48.00	79.11	87.25	97.57	75.88	<u>90.58</u>	<u>96.00</u>	77.50
13	CASE Pre-LaSCo.Ca. [†] [21]	49.35	80.02	88.75	<u>97.47</u>	<u>76.48</u>	90.37	95.71	<u>78.25</u>
14	Ours F	44.70	76.59	86.43	97.18	75.02	89.92	95.64	75.81
15	Ours R ₅₀	50.55	81.75	89.78	97.18	80.04	91.90	96.58	80.90

Table 2: CIRR, test split. We pick our best-performing model on the validation split and submit results online for testing. We report the Average Metric ($Recall@5 + Recall_{Subset}@1$)/2 as in [28]. Rows 1-8 are cited from [28]. †: Methods trained with additional pre-training data. **F** (shaded) denotes Candidate Filtering model, **R**_K denotes Candidate Re-ranking model with results obtained on the top-*K* filtered results from **F**. For CIRR we use top-50, which has a ground truth coverage of 97.18%. Best numbers (resp. second-best) are in **black** (resp. underlined).

Regarding our first stage filtering model (row 19), we achieve a performance slightly behind CASE. As discussed in Section 3, we share a similar BLIP-based architecture and training pipeline as CASE. Upon examining the ablation studies by Levy et al. [21], we conjecture that the lower performance is mainly because we adopt a different loss and do not finetune the ViT image encoder alongside due to hardware limits. We note that nevertheless, our re-ranked performance surpasses all existing methods by a large margin.

CIRR. Table 2 compares the performance on CIRR. Overall, we observe a similar trend in performance increase as in Fashion-IQ. This includes the performance comparison between our filtering

model (row 14) and CASE [21] (row 12), as discussed above. We notice that our re-ranked results (row 15) outperform all previous methods, including models that are based on BLIP and pre-trained on additional data of large scales (row 13). This demonstrates that our design more effectively harnesses the information within the input entities than existing work.

4.3 Ablation Study

In Table 3, we test several variants of the re-ranking model to verify our design choices. We report performance on the Fashion-IQ validation split for all experiments. Further ablations studies are included in Section B.

We begin with assessing the necessity of our dual-encoder setup, as shown in Table 3 row 1. We validate the need for the Encoder- z_t , as otherwise, the performance drops significantly. Building on the above, we further verify our use of z_t as a surrogate of I_R . As discussed in Section 3, Encoder- z_t is designed to allow for interactions between the reference and candidate images. However, GPU memory consumption prohibits direct image-image cross-attention, unless certain spatial pooling is applied to the reference image. In rows 2-3, we show that it is less desired to replace z_t with such pooled features, which, in turn, corroborates that z_t is a better alternative for the network.

We additionally show two variants related to our design choices. Row 4 replaces the first six merging layers from the average pooling to MLP, while row 5 removes the weight-sharing of the FF layers. We note a consistent performance decrease in both cases.

Methods	Dress		Shirt		Toptee		Average		Avg. Metric
	R@10	R@50	R@10	R@50	R@10	R@50	R@10	R@50	
Ours \mathbf{R}_{100}	48.14	71.34	50.15	71.25	55.23	76.80	51.17	73.13	62.15
1 w/o. z_t	37.48	66.83	39.16	65.75	46.25	72.62	40.96	68.40	54.68
2 w. Ref _{CLS}	46.55	71.24	47.84	70.07	54.36	75.83	49.59	72.38	60.98
3 w. Ref _{CLS} + Spatial-6×6	48.04	71.10	48.04	70.31	54.82	76.39	50.30	72.60	61.45
4 Full-MLP merge	47.00	70.80	47.79	69.63	54.61	76.54	49.80	72.32	61.06
5 Dual Feed-Forward	44.67	69.71	46.37	69.97	52.83	76.39	46.96	72.02	59.99

Table 3: Ablation studies on Fashion-IQ, validation split. Shaded is our Candidate Re-ranking model as in Table 1 row 20. Row 1 ablates the utility of the dual-encoder design. Rows 2-3 examine the difference between using z_t and the reference image features in Encoder- z_t in Figure 1. In row 3, we choose Ref_{CLS} + Spatial-6×6 to showcase the performance under minimum information loss with pooling, as the hardware cannot accommodate a longer sequence of image input. Rows 4-5 test architectural designs. See further ablations in Section B.2. Best results are in **black**.

4.4 Inference Time

One obvious limitation of our method is the inference time of the re-ranking model, as it requires exhaustive pairing of the query and top- K candidates. Several factors contribute to the case, including the size of the validation/test split of the dataset, choice of K , as well as the general length of the input text, which affects the efficiency of the attention layers within the transformer. We observe that compared to a traditional vector distancing-based method, e.g., our filtering model, the inference time of the re-ranking step is increased by approximately 8 times on Fashion-IQ and 35 times on CIRR. Qualitatively, it takes around 9 minutes (resp. 7 minutes) for inference on the validation split of Fashion-IQ (resp. CIRR). We note that our focus of this work is on achieving higher performance through model architectural design and better use of input information, and is not optimized towards e.g., industrial applications. Meanwhile, the additional cost results in a significant increase in performance — around 5% in average Recall compared to the filtering results (Table 1 and Table 2).

4.5 Qualitative Results

We present several retrieved results on CIRR in Figure 3, where we show the pipeline of filtering followed by re-ranking. For **(a)** and **(b)**, we note that explicit text-candidate pairing can be more beneficial in cases where new elements are added (i.e., “trees”, “two people” and “cat”), as the re-ranking model can readily identify concepts within each candidate, and assess its correlations

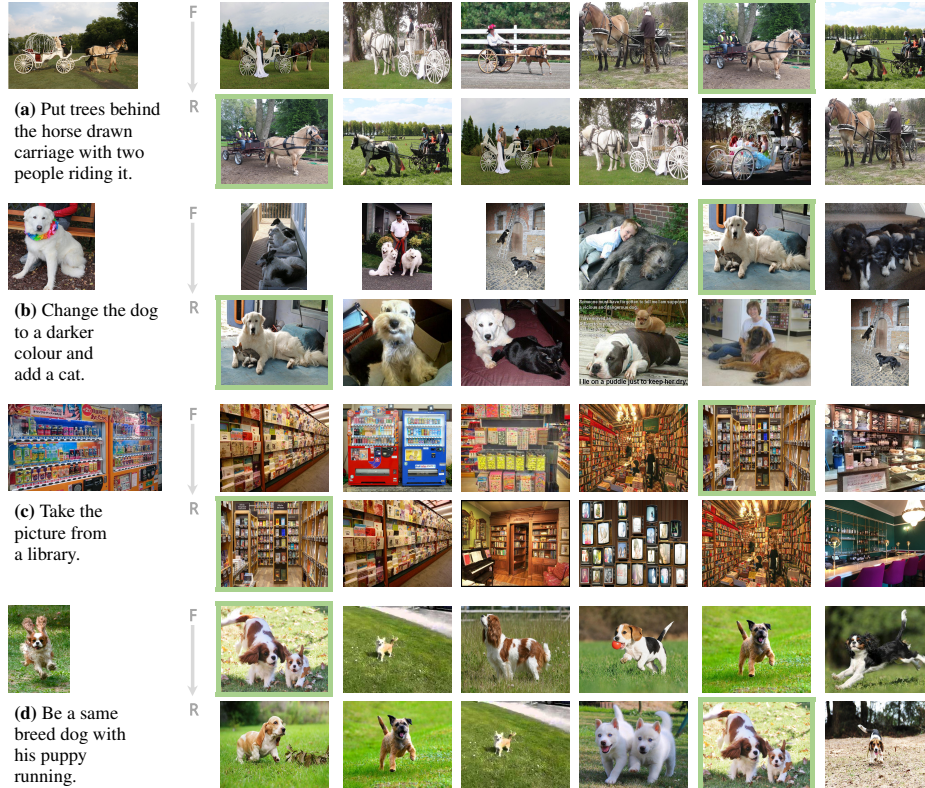


Figure 3: Qualitative examples on CIR. For each sample, we showcase the query (left) with the filtered top-6 candidates (F), followed by the re-ranked top-6 results (R). True targets are in green frames. We demonstrate three cases where re-ranking brings the true target forward (a-c), and one failure case (d). Note that the aspect ratio of certain candidate images are not preserved due to the page width limitation. Additional examples can be seen in the supplementary material.

between the text. We specifically point to (b), where with initial filtering, only one candidate among the top-6 contains a cat as the text describes. After re-ranking, three candidates with cat are brought forward, with the true target ranked the first. In (c), we show that our re-ranking model is also effective at recognizing global visual concepts such as scenes (i.e., library). Finally, we list a failure case of the re-ranking in (d), where we observe that our re-ranking model fails to associate the concept of “with” with having two entities simultaneously in the image. As a result, the top-3 re-ranked candidates each only pictures a single puppy running.

We additionally point out that the filtering module is effective at removing easy negatives. As shown in Figure 3, on each sample, the top-ranked candidates are already picturing similar objects or scenes as the reference. For more qualitative examples please see Section C.

5 Conclusion

We propose a two-stage method for composed image retrieval, which trades off the inference cost with a model that exhaustively pairs up queries with each candidate image. Our filtering module follows prior work and uses vector distances to quickly generate a small candidate set. We then design a dual-encoder architecture to assess the remaining candidates against the query for their relevancy. Both stages of our method are designed based on the existing vision-and-language pre-trained model. We experimentally show that our approach consistently outperforms existing methods on two popular benchmarks, Fashion-IQ and CIR.

6 Discussions

Social Impacts. Our method is a generic retrieval model that accepts user input and locates an already existing image. Therefore, it bears low potential negative social impacts. However, we point out that it is possible for a model trained on open-domain content sourced from, e.g., the Internet to exhibit certain biases. We note that such biases, as in other similar vision-and-language tasks, can be mitigated with a careful filtering of data, but nevertheless, still remains as an active area of research.

Limitations. The main limitation of our method is the inference speed, which is discussed in Section 4.4. Additionally, as mentioned above, our method might have inherent potential biases from BLIP, which is pre-trained on web-sourced image-text pairs [35].

References

- [1] P. Anderson, X. He, C. Buehler, D. Teney, M. Johnson, S. Gould, and L. Zhang. Bottom-up and top-down attention for image captioning and visual question answering. In *IEEE Conference on Computer Vision and Pattern Recognition*, 2018.
- [2] M. U. Anwaar, E. Labintceva, and M. Kleinsteuber. Compositional learning of image-text query for image retrieval. In *Proceedings of the IEEE/CVF Winter Conference on Applications of Computer Vision (WACV)*, January 2021.
- [3] A. Baldrati, M. Bertini, T. Uricchio, and A. Del Bimbo. Effective conditioned and composed image retrieval combining clip-based features. In *Proceedings of the IEEE/CVF Conference on Computer Vision and Pattern Recognition (CVPR)*, 2022.
- [4] A. Baldrati, M. Bertini, T. Uricchio, and A. Del Bimbo. Conditioned and composed image retrieval combining and partially fine-tuning clip-based features. In *Proceedings of the IEEE/CVF Conference on Computer Vision and Pattern Recognition (CVPR) Workshops*, 2022.
- [5] Y. Chen, S. Gong, and L. Bazzani. Image search with text feedback by visiolinguistic attention learning. In *IEEE Conference on Computer Vision and Pattern Recognition*, 2020.
- [6] Y.-C. Chen, L. Li, L. Yu, A. E. Kholly, F. Ahmed, Z. Gan, Y. Cheng, and J. Liu. Uniter: Universal image-text representation learning. In *European Conference on Computer Vision*, 2020.
- [7] O. Chum, J. Philbin, J. Sivic, M. Isard, and A. Zisserman. Total recall: Automatic query expansion with a generative feature model for object retrieval. In *2007 IEEE 11th International Conference on Computer Vision*, pages 1–8, 2007.
- [8] G. Couairon, M. Cord, M. Douze, and H. Schwenk. Embedding arithmetic for text-driven image transformation. *ArXiv*, abs/2112.03162, 2021.
- [9] G. Delmas, R. S. de Rezende, G. Csorika, and D. Larlus. Artemis: Attention-based retrieval with text-explicit matching and implicit similarity. In *International Conference on Learning Representations*, 2022.
- [10] J. Devlin, M.-W. Chang, K. Lee, and K. Toutanova. BERT: Pre-training of deep bidirectional transformers for language understanding. In *Proceedings of the 2019 Conference of the North American Chapter of the Association for Computational Linguistics: Human Language Technologies, Volume 1 (Long and Short Papers)*, pages 4171–4186, Minneapolis, Minnesota, June 2019. Association for Computational Linguistics.
- [11] E. Dodds, J. Culpepper, S. Herdade, Y. Zhang, and K. Boakye. Modality-agnostic attention fusion for visual search with text feedback. *ArXiv*, abs/2007.00145, 2020.
- [12] A. Dosovitskiy, L. Beyer, A. Kolesnikov, D. Weissenborn, X. Zhai, T. Unterthiner, M. Dehghani, M. Minderoeder, G. Heigold, S. Gelly, J. Uszkoreit, and N. Houlsby. An image is worth 16x16 words: Transformers for image recognition at scale. In *International Conference on Learning Representations*, 2021.
- [13] X. Guo, H. Wu, Y. Gao, S. J. Rennie, and R. Feris. The Fashion IQ Dataset: Retrieving images by combining side information and relative natural language feedback. *ArXiv*, abs/1905.12794, 2019.
- [14] X. Han, Z. Wu, P. X. Huang, X. Zhang, M. Zhu, Y. Li, Y. Zhao, and L. S. Davis. Automatic spatially-aware fashion concept discovery. In *IEEE International Conference on Computer Vision*, 2017.
- [15] X. Han, X. Zhu, L. Yu, L. Zhang, Y.-Z. Song, and T. Xiang. Fame-vil: Multi-tasking vision-language model for heterogeneous fashion tasks, 2023.
- [16] M. Hosseinzadeh and Y. Wang. Composed query image retrieval using locally bounded features. In *IEEE Conference on Computer Vision and Pattern Recognition*, 2020.
- [17] S. Jandial, P. Badjatiya, P. Chawla, A. Chopra, M. Sarkar, and B. Krishnamurthy. Sac: Semantic attention composition for text-conditioned image retrieval. In *2022 IEEE/CVF Winter Conference on Applications of Computer Vision (WACV)*. IEEE Computer Society, 2022.
- [18] J. Kim, Y. Yu, H. Kim, and G. Kim. Dual Compositional Learning in Interactive Image Retrieval. In *AAAI*, 2021.
- [19] J.-H. Kim, S.-W. Lee, D. Kwak, M.-O. Heo, J. Kim, J.-W. Ha, and B.-T. Zhang. Multimodal residual learning for visual qa. In *Advances in neural information processing systems*, 2016.

- [20] S.-M. Lee, D. Kim, and B. Han. Cosmo: Content-style modulation for image retrieval with text feedback. *2021 IEEE/CVF Conference on Computer Vision and Pattern Recognition (CVPR)*, 2021.
- [21] M. Levy, R. Ben-Ari, N. Darshan, and D. Lischinski. Data roaming and early fusion for composed image retrieval, 2023.
- [22] J. Li, R. R. Selvaraju, A. D. Gotmare, S. Joty, C. Xiong, and S. Hoi. Align before fuse: Vision and language representation learning with momentum distillation. In *NeurIPS*, 2021.
- [23] J. Li, D. Li, C. Xiong, and S. Hoi. Blip: Bootstrapping language-image pre-training for unified vision-language understanding and generation. In *ICML*, 2022.
- [24] J. Li, D. Li, S. Savarese, and S. Hoi. BLIP-2: bootstrapping language-image pre-training with frozen image encoders and large language models. In *ICML*, 2023.
- [25] W. Li, L. Duan, D. Xu, and I. W. Tsang. Text-based image retrieval using progressive multi-instance learning. In *IEEE International Conference on Computer Vision*, 2011.
- [26] X. Li, X. Yin, C. Li, X. Hu, P. Zhang, L. Zhang, L. Wang, H. Hu, L. Dong, F. Wei, Y. Choi, and J. Gao. Oscar: Object-semantics aligned pre-training for vision-language tasks. In *European Conference on Computer Vision*, 2020.
- [27] T.-Y. Lin, M. Maire, S. Belongie, J. Hays, P. Perona, D. Ramanan, P. Dollár, and C. L. Zitnick. Microsoft coco: Common objects in context. In *Computer Vision – ECCV 2014*, pages 740–755. Springer International Publishing, 2014.
- [28] Z. Liu, C. Rodriguez, D. Teney, and S. Gould. Image retrieval on real-life images with pre-trained vision-and-language models. In *IEEE International Conference on Computer Vision*, 2021.
- [29] Z. Liu, W. Sun, Y. Hong, D. Teney, and S. Gould. Bi-directional training for composed image retrieval via text prompt learning, 2023.
- [30] I. Loshchilov and F. Hutter. Decoupled weight decay regularization. In *International Conference on Learning Representations*, 2017.
- [31] I. Loshchilov and F. Hutter. SGDR: Stochastic gradient descent with warm restarts. In *International Conference on Learning Representations*, 2017.
- [32] E. Perez, F. Strub, H. de Vries, V. Dumoulin, and A. Courville. Film: Visual reasoning with a general conditioning layer, 2017.
- [33] A. Radford, J. W. Kim, C. Hallacy, A. Ramesh, G. Goh, S. Agarwal, G. Sastry, A. Askell, P. Mishkin, J. Clark, G. Krueger, and I. Sutskever. Learning transferable visual models from natural language supervision. In *Proceedings of the 38th International Conference on Machine Learning*, 2021.
- [34] A. Santoro, D. Raposo, D. G. Barrett, M. Malinowski, R. Pascanu, P. Battaglia, and T. Lillicrap. A simple neural network module for relational reasoning. In *Advances in neural information processing systems*, pages 4967–4976, 2017.
- [35] C. Schuhmann, R. Beaumont, R. Vencu, C. W. Gordon, R. Wightman, M. Cherti, T. Coombes, A. Katta, C. Mullis, M. Wortsman, P. Schramowski, S. R. Kundurthy, K. Crowson, L. Schmidt, R. Kaczmarczyk, and J. Jitsev. LAION-5b: An open large-scale dataset for training next generation image-text models. In *Thirty-sixth Conference on Neural Information Processing Systems Datasets and Benchmarks Track*, 2022.
- [36] X. Shen, Z. Lin, J. Brandt, S. Avidan, and Y. Wu. Object retrieval and localization with spatially-constrained similarity measure and k-nn re-ranking. In *2012 IEEE Conference on Computer Vision and Pattern Recognition*, pages 3013–3020, 2012.
- [37] A. Suhr, S. Zhou, A. Zhang, I. Zhang, H. Bai, and Y. Artzi. A corpus for reasoning about natural language grounded in photographs. *Proceedings of the 57th Annual Meeting of the Association for Computational Linguistics*, 2019.
- [38] S. Tong and E. Chang. Support Vector Machine active learning for image retrieval. In *Proceedings of the Ninth ACM International Conference on Multimedia*, 2001.
- [39] S. Vaze, N. Carion, and I. Misra. Genecis: A benchmark for general conditional image similarity. In *Proceedings of the IEEE/CVF Conference on Computer Vision and Pattern Recognition*, 2023.
- [40] N. Vo, L. Jiang, C. Sun, K. Murphy, L.-J. Li, L. Fei-Fei, and J. Hays. Composing text and image for image retrieval - an empirical odyssey. In *IEEE Conference on Computer Vision and Pattern Recognition*, 2019.
- [41] H. Wen, X. Song, X. Yang, Y. Zhan, and L. Nie. Comprehensive linguistic-visual composition network for image retrieval. In *Proceedings of the 44th International ACM SIGIR Conference on Research and Development in Information Retrieval*, SIGIR '21, page 1369–1378. Association for Computing Machinery, 2021.
- [42] Y. Yang, M. Wang, W. gang Zhou, and H. Li. Cross-modal joint prediction and alignment for composed query image retrieval. *Proceedings of the 29th ACM International Conference on Multimedia*, 2021.
- [43] Y. Yu, S. Lee, Y. cheol Choi, and G. Kim. Curlingnet: Compositional learning between images and text for fashion iq data. *ArXiv*, 2020.
- [44] C. Zhang, J. Y. Chai, and R. Jin. User term feedback in interactive text-based image retrieval. *Proceedings of the 28th Annual International ACM SIGIR Conference on Research and Development in Information Retrieval*, 2005.
- [45] H. Zhu, Y. Wei, Y. Zhao, C. Zhang, and S. Huang. Amc: Adaptive multi-expert collaborative network for text-guided image retrieval. *ACM Trans. Multimedia Comput. Commun. Appl.*, 2023.

Supplementary Material

A Implementation Details

Here, we detail the hyperparameters we use for training in the two stages. We follow Li et al. [23] in initializing the transformer encoders, as mentioned in Section 4.1.

For all models in both stages, we use AdamW [30] with an initial learning rate of 2×10^{-5} , a weight decay of 0.05, and a cosine learning rate scheduler [31] with its minimum learning rate set to 0. Image resolution is set to 384×384 following Li et al. [23].

For Candidate Filtering (first stage) model, we train with a batch size of 512 for 10 epochs on both Fashion-IQ [13] and CIRR [28]. For Candidate Re-ranking (second stage) model, we reduce the batch size to 16 due to the GPU memory limit, as it requires exhaustively pairing up queries with each candidate. We use a single NVIDIA A100 80G for all our experiments. For Fashion-IQ, we train the re-ranking model for 50 epochs, for CIRR, we train it for 80 epochs.

B Additional Ablation Study

B.1 K values in Re-ranking

Table 4 and Table 5 studies the effect of K for the re-ranking model. Recall that K is the number of samples taken from the first stage to be re-ranked. As discussed in Section 3.3, K only affects inference but not training.

Given that increasing K effectively increases the ground truth coverage (defined in Section 3.1), one could reasonably expect that a larger K yields higher performance. However, we note that a higher K would also lead to more negative candidates, which potentially impact the performance should the re-ranking model fails to properly rank them.

For Fashion-IQ, we see a general trend of performance increase while increasing K , except for when $K = 200$ (Table 4 row 7). For CIRR (Table 5), we observe minor performance differences when varying K , which is unsurprising given the high ground truth coverage in general. Consequently, we could only notice a clear trend in Recall@50. Here, we note that K does not affect validating on Recall_{Subset}, as such a metric only concerns five pre-determined candidates per query.

As discussed in Section 3.1, we have not handpicked K per training instance. Instead, for every dataset, we globally select K based on the balance between the ground truth coverage and inference cost.

Methods	Dress		Shirt		Toptee		Average		Avg. Metric
	R@10	R@50	R@10	R@50	R@10	R@50	R@10	R@50	
1 F	43.78	67.38	45.04	67.47	49.62	72.62	46.15	69.15	57.65
2 R₅₀	48.24	67.38	50.15	67.47	54.56	72.62	50.98	69.15	60.07
3 R₇₀	48.14	69.66	50.59	69.09	54.87	75.83	51.20	71.52	61.36
4 R₉₀	48.14	70.90	50.15	70.76	55.07	76.13	51.12	72.60	61.86
5 R₁₀₀	48.14	71.34	50.15	71.25	55.23	76.80	51.17	73.13	62.15
6 R₁₅₀	48.09	71.49	50.20	71.49	55.28	77.41	51.19	73.46	62.33
7 R₂₀₀	47.89	71.44	50.15	71.00	55.38	77.41	51.14	73.28	62.21

Table 4: Fashion-IQ, validation split. Ablation on K value in Candidate Re-ranking. **F** (row 1): the Candidate Filtering model (attached as a reference to compare against), as in Table 1 row 19. Shaded: our choice of K when reporting the main results in Table 1 row 20.

B.2 Ablation Study in CIRR

Table 6 shows the ablation studies conducted on CIRR, which complements the same set of experiments performed on Fashion-IQ in Table 3. We conclude that reference images play an equally important role in CIRR (row 1) as in Fashion-IQ, and that our choice of using z_t as a surrogate for it is validated (row 2). Regarding the ablated design choices of the architecture, we notice they

Methods	Recall@ K				Recall _{Subset} @ K			Avg.
	$K = 1$	$K = 5$	$K = 10$	$K = 50$	$K = 1$	$K = 2$	$K = 3$	Metric
1 F	46.83	78.59	88.04	97.08	76.11	90.65	96.05	77.53
2 R ₃₀	53.03	83.16	90.62	95.26	80.44	92.54	97.01	81.80
3 R ₄₀	52.98	82.83	90.29	96.27	80.44	92.54	97.01	81.64
4 R ₅₀	53.24	83.11	90.03	97.08	80.44	92.54	97.01	81.78
5 R ₁₀₀	52.88	82.92	90.07	97.90	80.44	92.54	97.01	81.68
6 R ₁₅₀	52.91	82.85	90.05	98.04	80.44	92.54	97.01	81.65

Table 5: CIRR, validation split. Ablation on K value in Candidate Re-ranking. **F** (row 1): the Candidate Filtering model (attached as a reference to compare against), as in Table 2 row 14. Shaded: our choice of K when reporting the main results in Table 2 row 15. Note the values differ for the test and validation splits.

bear a slightly smaller impact on CIRR than on Fashion-IQ, but our design still yields better overall performance in the Recall_{Subset} and Average Metric.

Interestingly, we discover that the Recall_{Subset} performance does not suffer much without the reference image (row 1), as opposed to in Fashion-IQ. Indeed, previous work [21, 28, 39] observe a similar case in their ablation studies. This is thought to be caused by the fact that Recall_{Subset} only considers a selected group of five candidates of high similarities, hence the information within the reference image contributes less to the retrieval.

Methods	Recall@ K				Recall _{Subset} @ K			Avg.
	$K = 1$	$K = 5$	$K = 10$	$K = 50$	$K = 1$	$K = 2$	$K = 3$	Metric
Ours R ₅₀	53.24	83.11	90.03	97.08	80.44	92.54	97.01	81.78
1 <i>w/o. z_t</i>	43.51	75.25	84.24	97.08	80.34	91.68	96.72	77.79
2 <i>w. Ref_{CLS} + Spatial-6×6</i>	52.98	83.23	90.48	97.08	79.55	90.06	96.70	81.39
3 Full-MLP merge	52.91	82.64	90.15	97.08	79.60	92.25	96.89	81.12
4 Dual Feed-Forward	54.20	82.80	90.39	97.08	80.22	91.89	96.53	81.51

Table 6: Ablation studies on CIRR, validation split. Experiments conducted following Table 3 on Fashion-IQ. Row 1 ablates the utility of the dual-encoder design. Rows 2 examines the difference between using z_t and the reference image features in Encoder- z_t . Recall that z_t is pre-computed from the previous stage using the reference image and text (Figure 1). We choose Ref_{CLS} + Spatial-6×6 to showcase the performance under minimum information loss with pooling, as the hardware cannot accommodate a longer sequence of image input. Rows 3-4 test architectural designs. Row 3 replaces the first six merging layers from the average pooling to MLP, while row 4 removes the weight-sharing of the FF layers. Shaded is our Candidate Re-ranking model as in Table 2 row 15. Note the values differ for the test and validation splits.

C Additional Qualitative Results

Figure 4 provides qualitative examples of Fashion-IQ, with the layout following Figure 3. We illustrate both success and failure cases for our re-ranking model.



Figure 4: Qualitative examples on Fashion-IQ. For each sample, we showcase the query (left) with the filtered top-6 candidates (F), followed by the re-ranked top-6 results (R). True targets are in green frames. For examples with ground truth initially ranked beyond the top-6, we report their rankings below the annotation. We demonstrate cases where re-ranking brings the ground truth forward, along with failure cases. Note the sometimes ambiguous and abstract human annotations, as well as the existence of false negatives (due to the high similarities among cloth images). Collectively, this makes Fashion-IQ challenging, which demonstrates the power of our re-ranking stage.